MAGIC-TDAS 02-04
020401/MGaug

Calibration Analysis for the MAGIC Telescope

Markus Gaug, Thomas Schweizer
<markus@ifae.es>, <tschweiz@ifae.es>

May, 2002

Abstract

After the implementation and testing of the calibration system, a full analysis software needs to be written. This document gives the status of the implementation of the system into the surrounding software and defines what an analysis of the obtained data should consist of. A more detailed calculation of the total excess noise of the telescope is introduced and dependencies on high-voltage, photon wavelength and incidence angles are examined. We suggest to calibrate in photons instead of photo-electrons and to install a light source on the Roque de las Muchachos in order to calibrate the telescope as a whole including the mirrors and the effect of different photon incidence angles. Finally, a short description of the calibration steering software is given.

Contents

1 Introduction

At the Barcelona meeting, the implementation of the MAGIC calibration system was presented [1]. The hardware and the steering software are at the point of being finished, however the software to analyze and use it for the operation of the telescope still have to implemented.

A calibration consists of measuring the response of the whole light-detection and amplification chain to a precisely known (mono-chromatic) light flux. In the case of the MAGIC calibration system (and for the pulse mode), the former will be the fluency of (to first approximation mono-chromatic) photons N_γ emitted during 3–4 ns by an assembly of synchronized LEDs which emit light in three different colours (green $\equiv$ 520 nm, blue $\equiv$ 460 nm and UV $\equiv$ 370 nm). See [2] for the complete setup. The photons hit the geometrical area of the *Winston cones*. The detector response consists of an output pattern of the different time slices in the FADC. For the moment, detailed FADC studies are not yet at hand to the point that we know how to best extract the time information. [3] proposes to take the mean and the width of the FADC time slices to get some time calibration. However, the level-1 trigger should already monitor a 2-5ns simultaneity just because of the coincidence requirement [4]. We will further assume that we use an adequate overall FADC charge integral Q and incorporate the time information at a later stage.

After taking the corresponding calibration runs, we obtain a charge distribution f with a pedestal peak at Q_0, a signal peak at Q_μ and the corresponding variances σ_0^2 and σ^2. The result can then be written as:

$$P_\gamma(\lambda) \equiv \frac{f\Big((Q_\mu - Q_0), \sigma_0, \sigma\Big)}{N_\gamma} = \epsilon_W(\theta) \otimes \epsilon_{QE}(\lambda) \otimes \epsilon_{coll}(U_{\mathsf{HV}}) \otimes P_{PhE}(U_{\mathsf{HV}}) \tag{1}$$

Eq. (1) defines the conversion *probability function* P_γ for an incident photon of wavelength λ to a probability distribution of measured charges. (The symbol $\otimes$ means that the single probability functions have to be folded into each other.) They consist of the collection efficiency of the Winston cones $\epsilon_W(\theta)$ which depends mostly on the incident angle θ of the photon with respect to the main axis of the photomultiplier. This dependency gives a much larger effect for the MAGIC telescope than for the old CT1 system and varies about 30%. Furthermore, the quantum efficiency of the photo-cathode $\epsilon_{QE}(\lambda)$ which depends in first order on the photon wavelength, and the collection efficiency of a photo-electron to hit the first dynode $\epsilon_{coll}(U_{\mathsf{HV}})$ depending mainly on the high voltage setting. The MAGIC pixels, however will have a fixed voltage between the first and second dynode, thus this dependency vanishes. The last term in eq. (1) gives the conversion probability function P_{Phe} from the photo-electron to a measured charge Q.

The functions $\epsilon_W(\theta)$, $\epsilon_{QE}(\lambda)$ and ϵ_{coll} are to a first approximation *binomial distributions* W_η^n with each a mean $\mu = n \cdot \eta$ and a variance $\sigma^2 = n \cdot \eta(1-\eta)$ where n denotes the number of photons *incident* to the corresponding function and η the single photon transmission probability [1]. The three functions can be convoluted and yield:

$$W^{N_\gamma}_{\eta_W,\eta_{QE},\eta_{coll}}(k) \equiv W^{N_\gamma}_{\eta_{tot}}(k) = \sum_{k'=0}^{N_\gamma} \sum_{\substack{k''=0 \\ k\leq k''}}^{k'} W^{N_\gamma}_{\eta_W}(k') \cdot W^{k'}_{\eta_{QE}}(k'') \cdot W^{k''}_{\eta_{coll}}(k) \tag{2}$$

[1] This is not exactly true for the Winston cones since they increase the quantum efficiency of the PMTs by increasing the conversion probability for once transmitted photons.

with a mean:

$$\overline{N}_{PhE}(\lambda,\theta) = N_\gamma \cdot \eta_W(\theta) \cdot \eta_{QE}(\lambda) \cdot \eta_{coll} \equiv N_\gamma \cdot \eta_{tot}(\lambda,\theta) \tag{3}$$

and a variance:

$$\mathsf{Var}(k;\lambda,\theta) = N_\gamma \cdot \eta_{tot}(\lambda,\theta)\Big(1 - \eta_{tot}(\lambda,\theta)\Big) \tag{4}$$

Note the dependencies on wavelength, incident angle and HV-setting of the mean and the variance.

The probability function P_{Phe} is a convolution of several Poissonians from the amplification in the PMT, the contribution of backscattered electrons from the first dynode and further amplification and noise in the electronic and optical chain.

For low fluencies of photo-electrons Q_μ during the time gate of the amplification chain, a Poisson-distribution of k photons per trigger is obtained with a Gaussian smearing of each charge value. For many consecutive events, we get a superposition of all Gaussians with Poissonian amplitudes:

$$P(Q,\overline{N}_{PhE},k;Q_k,\sigma_k) = \frac{e^{-\overline{N}_{PhE}} \cdot \overline{N}^{\,k}_{PhE}}{k!} \cdot \frac{e^{-\frac{(Q-Q_k)^2}{2\sigma_k^2}}}{\sigma_k\sqrt{2\pi}} \tag{5}$$

In the case of high photon fluxes ($\overline{N}_{PhE} \gtrsim 10$), the Gaussians in eq. (5) cannot be resolved any more and an ordinary Poisson distribution would be more adequate to fit. However, in this limit the Poisson can be replaced by a Gaussian distribution with a mean $\overline{Q}$:

$$P(Q,\overline{Q}) = \frac{e^{-\frac{(Q-\overline{Q})^2}{2\overline{Q}}}}{\sqrt{2\pi\overline{Q}}} \tag{6}$$

We can now define the mean conversion factor $\overline{C}_{PhE}$ which converts photo-electrons into charges:

$$\overline{C}_{PhE}(U_{\mathsf{HV}}) \equiv \overline{G}(U_{\mathsf{HV}}) \cdot \overline{A} = \frac{\overline{Q}(U_{\mathsf{HV}})}{\overline{N}_{PhE}} \tag{7}$$

It consists of the average gain $\overline{G}$ of the PMT multiplied with the gain of the further electronic and optical link amplification $\overline{A}$. For the CT1 system, these conversion factors were used to "flat-field" the camera. This means that the high-voltages of every PMT were adjusted so that every $\overline{C}_{PhE}$ got the same value and a later analysis could calculate the total number of photo-electrons in a straight-forward way.

Additionally, an excess noise factor F_{PhE} can be defined[2]:

$$\begin{aligned} F_{PhE}(U_{\mathsf{HV}}) = \frac{\mathsf{var}(Q)}{\mathsf{var}(N_{PhE})} &= \overline{C}^{-2}_{PhE}(U_{\mathsf{HV}}) \cdot \frac{\mathsf{Var}(Q)}{\mathsf{Var}(N_{PhE})} \\ &\approx \mathsf{var}(Q) \cdot \overline{N}_{PhE} \end{aligned} \tag{8}$$

where we have used the definition of the fractional variance $\mathsf{var}(X) \equiv \frac{\mathsf{Var}(X)}{\overline{X}^2}$ and $\sigma_{PhE} \approx \sqrt{\overline{N}_{PhE}}$ which is true for $N_{PhE} \gtrsim 10$. Note that F_{PhE} does not depend on the wavelength or incident angles since it is a property of the electronic amplification chain alone. Replacing the probability function $f\Big((Q_\mu - Q_0),\sigma,\sigma_0\Big)$ in eq. (1) by the simple mean $\overline{Q}$, we get the mean conversion factor $\overline{C}_\gamma$ converting the numbers of photons into charges:

$$\overline{C}_\gamma(\lambda,\theta,U_{\mathsf{HV}}) \equiv \frac{\overline{Q}(\lambda,\theta,U_{\mathsf{HV}})}{N_\gamma} = \eta_{tot}(\lambda,\theta) \cdot C_{PhE}(U_{\mathsf{HV}}) \tag{9}$$

[2] Note that this definition differs from that used in [5] by the square root, i.e. $\sqrt{F_{PhE}}$(this paper) $\equiv F_{PhE}$([5]).

Note that this conversion factor (in contrast to $\overline{C}_{PhE}$) depends also on the wave-length and the incidence angle of the photon.

An overall excess noise factor F_{tot} can be defined via:

$$\begin{aligned}
F_{tot}(\lambda,\theta,U_{\mathsf{HV}}) = \frac{\mathsf{var}(Q)}{\mathsf{var}(N_\gamma)} &= \overline{C}_\gamma^{-2}(\lambda,\theta,U_{\mathsf{HV}}) \cdot \frac{\mathsf{Var}(Q)}{\mathsf{Var}(N_\gamma)} \\
&= \mathsf{var}(Q) \cdot N_\gamma \\
&\approx \frac{F_{PhE}(U_{\mathsf{HV}})}{\eta_{tot}(\lambda,\theta)}
\end{aligned} \tag{10}$$

where we have used eq. (3) and $\sigma_{N_\gamma} = \sqrt{N_\gamma}$. The last approximation in eq. (10) is a 0^{th} order one and will be treated in more detail in the next page.

At this place, an important systematic difference between light from the calibration box and air showers comes into play: Assuming that the Cherenkov light is in first order uniform over the telescope area and parallel to the telescope axis, we obtain a probability distribution function for the angle θ under which a photon arrives on the Winston cone:

$$P(\cos(\theta)) = \begin{cases} 0 & \frac{4D^2-R^2}{4D^2+R^2} > \cos(\theta) \\ -\frac{4D^2}{\pi R^2} \cdot \frac{1}{(1+\cos(\theta))^2} & 1 > \cos(\theta) > \frac{4D^2-R^2}{4D^2+R^2} \end{cases} \tag{11}$$

The complete derivation of eq. (11) is given in the appendix A. Figure 1 displays the shape of eq. 11 as well as the integral. Note that eq. 11 is normalized to $1/2\pi$.

Calibrating the total quantum efficiency with respect to air showers, one will thus have to fold the distribution of incidence angles with the single quantum efficiencies $\eta_{tot}(\theta)$. The corrected mean transmission probability η_{tot}^{corr} can be written in first order as follows:

$$\begin{aligned}
\eta_{tot}^{corr}(\lambda) &= \int_{\textbf{mirror disk}} P\big(\cos(\theta)\big) \cdot \eta_{tot}\big(\cos(\theta),\phi,\lambda\big)\; d\Omega \\
&= \int_0^{2\pi}\int_1^{\cos(\theta_{max})} P\big(\cos(\theta)\big) \cdot \eta_{tot}\big(\cos(\theta),\phi,\lambda\big)\; d\cos(\theta)\, d\phi \\
\mathsf{var}\big(\eta_{tot}^{corr}(\lambda)\big) &= \int_0^{2\pi}\int_1^{\cos(\theta_{max})} P\big(\cos(\theta)\big) \cdot \mathsf{var}\Big(\eta_{tot}\big(\cos(\theta),\phi,\lambda\big)\Big)\; d\cos(\theta)\, d\phi
\end{aligned} \tag{12}$$

The term $\cos(\theta_{max})$ has been derived as $\frac{4D^2-R^2}{4D^2+R^2}$ and its value is approximately 0.88 for MAGIC. This corresponds to a maximum incident angle of about 28° onto the Winston cones. Note that the transmission probabilities $\eta_{tot}\big(\cos(\theta),\phi,\lambda\big)$ are still unknown due to a lack of exact understanding of the behaviour of the Winston cones. Their values will be measured at IFAE and consequently used by the camera simulation software.

Whenever the calibration system obtains a transmission probability $\eta_{tot}(\lambda) \equiv \eta_{tot}(\theta_\perp,\lambda)$, it has to be multiplied with a correction function to S^{corr} in order to get the response of the whole system including the mirrors.

$$S^{corr}(\lambda) = \frac{\eta_{tot}^{corr}(\lambda)}{\eta_{tot}(\theta_\perp,\lambda)} \tag{13}$$

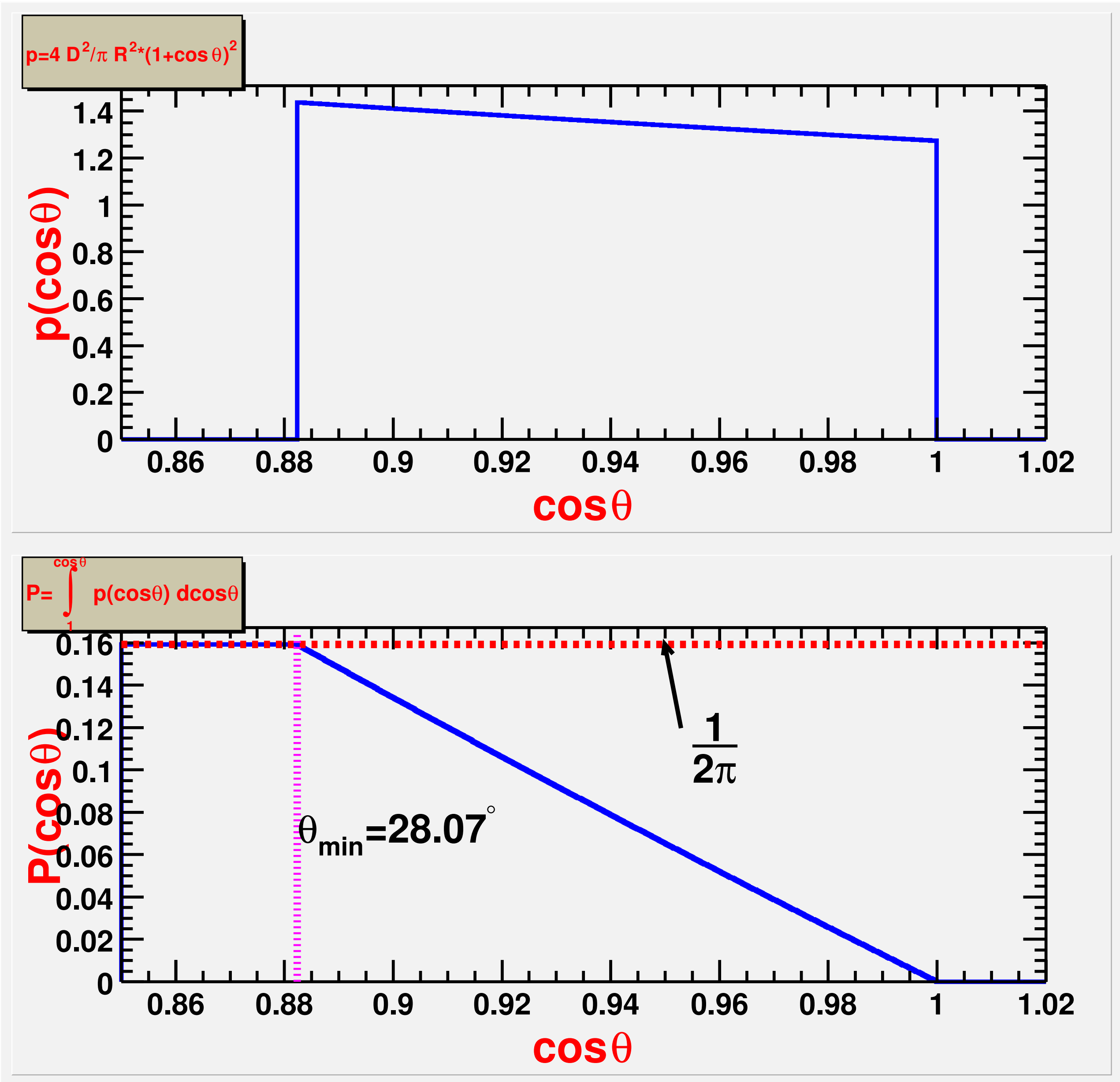

Figure 1: Shape of eq. 11

$S^{corr}(\lambda)$ will be measured at IFAE with the three LED colours available from the calibration system. Air showers also yield a different excess noise factor:

$$
\begin{aligned}
F_{tot}^{air\ sh.}(\lambda, U_{\mathsf{HV}}) = \frac{\mathsf{var}(Q;\lambda,U_{\mathsf{HV}})}{\mathsf{var}(N_\gamma^{air\ sh.})} &= \mathsf{var}(Q;\lambda,U_{\mathsf{HV}}) \cdot N_\gamma^{air\ sh.} \\
&\approx \frac{F_{PhE}(U_{\mathsf{HV}})}{\eta_{tot}^{corr}(\lambda)} \\
&\approx \frac{F_{tot}^{calib}(\lambda, U_{\mathsf{HV}})}{S^{corr}(\lambda)}
\end{aligned}
\tag{14}
$$

Again, the last two approximations are only of 0^{th} order.

In order to derive an expression for $F_{tot}^{air\ sh.}(\lambda, U_{\mathsf{HV}})$ analytically, we will first calculate the fractional variance of Q under the assumption that the photons arrive only from one single direction (e.g. using the calibration system):

$$
\begin{aligned}
\mathsf{var}^{calib}(Q;\lambda,U_{\mathsf{HV}}) &= \mathsf{var}(N_\gamma) + \\
&+ \frac{\big(1-\eta_{tot}(\lambda)\big)}{\overline{N}_\gamma \cdot \eta_{tot}(\lambda)} + \\
&+ \frac{\mathsf{var}(G(U_{\mathsf{HV}}))}{\overline{N}_\gamma \cdot \eta_{tot}(\lambda)} + \\
&+ \frac{\mathsf{var}(A)}{\overline{N}_\gamma \cdot \eta_{tot}(\lambda) \cdot \overline{G}(U_{\mathsf{HV}})}
\end{aligned}
\tag{15}
$$

For a complete derivation and detailed explications of the processes implied, see [5]. If the light source has a Poisson variance (which is valid for the LED and LONS light), i.e. $\mathsf{var}(N_\gamma) = 1/\overline{N}_\gamma$, eq. (15) reduces to:

$$
\mathsf{var}^{calib}(Q;\lambda,U_{\mathsf{HV}}) = \frac{1}{\overline{N}_{PhE}(\lambda, U_{\mathsf{HV}})} \cdot \Big(\ 1 + \mathsf{var}\big(G(U_{\mathsf{HV}})\big) + \frac{\mathsf{var}(A)}{\overline{G}(U_{\mathsf{HV}})}\ \Big)
\tag{16}
$$

The general definition of the excess noise factor of a PMT F_{PMT} then reads:

$$
F_{PMT}(U_{\mathsf{HV}}) = 1 + \mathsf{var}\big(G(U_{\mathsf{HV}})\big)
\tag{17}
$$

which equals F_{PhE} (eq. (8)) in the limit $\frac{\mathsf{var}(A)}{\overline{G}} \to 0$. This definition has been used in previous analyses and its values are currently being measured for 24 "well-calibrated" PMTs in Munich [7].

Ref. [5] shows that in the case of a photon detection efficiency $\eta_{tot}(\theta,\phi)$ which varies under the position on the cathode and under which angle θ a photo-electron is kicked out, eq. (16) gets an additional terms. The fractional variance for the signal with respect to air showers becomes therefore larger:

$$
\mathsf{var}^{air\ sh.}(Q;\lambda,U_{\mathsf{HV}}) = \mathsf{var}(\eta_{tot}^{corr}(\lambda)) + \frac{1}{\overline{N}_{PhE}(\lambda, U_{\mathsf{HV}})} \cdot \Big(\ 1 + \mathsf{var}\big(G(U_{\mathsf{HV}})\big) + \frac{\mathsf{var}(A)}{\overline{G}(U_{\mathsf{HV}})}\ \Big)
\tag{18}
$$

The full excess noise factor F_{tot} is related to F_{PMT} in the following way:

$$
\begin{aligned}
F_{tot}^{air\ sh.}(\lambda, U_{\mathsf{HV}}) &= F_{PMT}(U_{\mathsf{HV}}) \cdot \frac{1}{\eta_{tot}^{corr}(\lambda)} + \overline{N}_\gamma \cdot \Big(\ \mathsf{var}\big(\eta_{tot}^{corr}(\lambda)\big) + \frac{\mathsf{var}(A)}{\overline{G} \cdot \overline{N}_{PhE}} \ \Big) & (19) \\
&= \overline{N}_\gamma \cdot \mathsf{var}\big(\eta_{tot}^{corr}(\lambda)\big) + \frac{1}{\eta_{tot}^{corr}(\lambda)} \cdot \Big(\ F_{PMT}(U_{\mathsf{HV}}) + \frac{\mathsf{var}(A)}{\overline{G}} \ \Big) & (20) \\
&= \overline{N}_\gamma \cdot \mathsf{var}\big(\eta_{tot}^{corr}(\lambda)\big) + \frac{F_{tot}^{calib}(\lambda, U_{\mathsf{HV}})}{S^{\,corr}(\lambda)} & (21)
\end{aligned}
$$

Eq. (20) consists of three terms:

The variance of transmission probabilities under different incident angles on the PMT: $\mathsf{var}\big(\eta_{tot}^{corr}(\lambda)\big)$ (eq. (12)) will not be measured by the calibration system, but instead during the camera tests in the lab at IFAE. For the calibration runs at La Palma, this part must be added as an external number for each PMT. In principle, this variance can be made very small by accurate measurements, however its value will vary with time due to environmental effects. Moreover, it will be impossible to monitor it with the calibration system since it covers only one single incidence angle. In order to perform a survey of the stability of $\mathsf{var}(\eta_{tot}^{corr})$ from time to time, we suggest an external light source at the Roque de los Muchachos which allows a measurement of $S^{corr}(\lambda)$ and a detailed calibration of the whole system mirrors-camera. The arrival directions of light will look much like those from air showers which the telescope is pointing to. The telescope could focus on every pixel individually which would allow a more precise calibration to a known light flux (see also section (7)).

The excess noise factor of the PMT: The calibration system on the contrary is only able to measure the combination of this term together with the variance of the further amplification chain (see eq. (21)). Additionally, due to ageing effects of the dynodes, the gain at a given HV will diminished. We foresee to continuously adjust the total HV in order to keep the gain stable with time. This procedure will, however, effect the excess noise which will tend to increase.

The excess noise of the further amplification: This factor should be very small because of the high value of $\overline{G}$. However, the optical links could make a significant contribution, especially if long-term variations are concerned. For the "well-calibrated PMTs", an estimate can be drawn for the amount of excess noise imported by this third term. Assuming that F_{PMT} did not change too much since the lab measurements, it can be subtracted from the measured excess noise F_{tot}^{calib}.

We emphasize that the whole eqs. (20) and (21) are more elaborate than that used in previous analyses and perhaps with time we may realize that some terms may indeed be neglected. On the other side, the PMT construction including the Winston cones as well as the larger solid angle covered by the mirror area and the usage of the optical links introduce a different and partly not yet completely understood excess noise behaviour. For the moment, we suggest to take all terms into consideration, especially to control and monitor them.

2 The Calibration System

2.1 Overview of the Main Components

The main components of the calibration system as outlined in [2] are:

An LED pulser board: A variable number of LEDs in the three colours 370nm, 460nm, 520nm can be fired simulaneously with a pulse width of 3∼4 ns in the direction of the camera. Just above the the LEDs is situated a diffuser glass which makes the light flux uniform in an opening angle of $\sim 4°$. The board together with the steering elements is situated in a water-tight calibration box at the center of the mirror disk.

A continuous light source LED: Situated beside the pulser LEDs and also under the diffuser glass, it can supply 256 different light intensities.

A PIN-diode: Placed ∼1 m above the pulse LED at an opening angle of $\sim 3°$, it will calibrate the light flux emitted by the pulse LEDs. The PIN-diode itself is calibrated by an Americium-241 source housed in the same box.

A blind pixel: An EMI-9116A will be housed in one of the holes for the outmost ring of (large) PMTs and obscured by a 1/100-filter. It is amplified a BCAL-amplifier and its high-voltage can be set individually. There is space made available for a later mount of three independent "blind pixel" boxes situated just outside the ring of outmost pixels. This PMT will be able to resolve the single photo-electron peak.

2.2 The Calibration Schemes

The Calibration system will provide the following (flagged) calibration schemes:

Pedestal events for the PIN-diode: These events must be fitted to a Gaussian and thus yield: $Q_0^{Diode}, \Delta Q_0^{Diode}$, $\chi_0^{2\ Diode}$. We suggest to calculate as well a simple mean $\overline{Q}^{Diode}$ with a variance $\overline{(Q-\overline{Q})^2}$ in order to control possible outliers which would increase $\frac{\overline{Q}^{Diode}}{Q_0^{Diode}}$.

Pedestal events for each PMT: : Pedestal train runs are taken continuously at an initially proposed rate of 5 Hz and give a pedestal distribution for each PMT channel of the camera. A Gaussian will be fit to these distributions to obtain: $Q_0^{PMT}, \Delta Q_0^{PMT}, \sigma_0^{PMT}, \Delta\sigma_0^{PMT}, \chi_0^{2\ PMT}$ (and again $\overline{Q}_0^{PMT}$ and $\overline{(Q-\overline{Q})^2}$). Additionally, all pedestal events for the PIN-diode yield equivalent pedestal events for each PMT and vice-versa.

Events triggered by the Am-source in the PIN-diode box: These events will be taken continuously at a rate of $\sim 10^{-1}$Hz: Although the original distribution of electron energies is not Gaussian but follows a Lorentz distribution, electronic noise smears out the obtained distribution which consequently can be fitted to a Gaussian with good accuracy and yields: $Q_\mu^{Am}, \Delta Q_\mu^{Am}, \chi^{2\ Am}$. The mean Q_μ^{Am} corresponds to 59.5 keV $\equiv$ 16570 photo-electrons. Again, we propose to calculate simple mean values and variances in order to control possible outliers.

Events triggered by the pulse LEDs: Events of each of the three different colours (370nm, 460nm and 520nm) (or further combinations of colours) can be provided. A more detailed analysis will be given in section 2.3.

Linearity calibration: Eq's (9) and (10) are defined in a way which should not depend on the light intensity. It means that a linear behaviour of the amplification chain is expected. We know however, that especially the optical links may introduce non-linear behaviour. That's why for each of the three wavelength LEDs, different light intensities can be chosen and used for a linearity calibration of $\overline{C}_\gamma(N_\gamma)$, $\Delta C_\gamma(N_\gamma)$, $F_{tot}(N_\gamma)$, $\Delta F_{tot}(N_\gamma)$.

Events from the continuous light source: The continuous light source can provide 256 intensities. The number of photons arriving during a trigger time interval which follows a Poisson distribution characterized by a mean $< N_\gamma >$. The calibration will use about 20 steps of each 10.000 pedestal events. The events of each step can to a good approximaiton be fitted to a Gaussian and yield $Q_\mu(< N_\gamma >)$, $\Delta Q_\mu(< N_\gamma >)$, $\sigma_Q(< N_\gamma >)$, $\Delta\sigma_Q(< N_\gamma >)$ and a $\chi^2(< N_\gamma >)$. There is a relationship between the DC current I and the RMS noise σ_Q in the amplification chain due to the Poisson distributed nature of the LONS and the electronic noise σ_0:

$$(\sigma_Q^2 - \sigma_0^2) \propto I \tag{22}$$

Eq. (22) has always been assumed, but never calibrated. With the continuous light source, one can directly calibrate the exact dependency of σ_Q^2 vs. I for each pixel individually and thus more exactly monitor the pedestal RMS via measurements of the DC current.

2.3 Analysis of the Pulse LEDs Signals

The light coming from the pulse LEDs will yield signals in the following components:

PIN-diode: Again, the charge distribution must be fitted to a Gaussian to provide: $Q_\mu^{Diode}(\lambda), \Delta Q_\mu^{Diode}(\lambda)$, $\chi_Q^{2\ Diode}(\lambda)$ (and again $\overline{x}^{Diode}(\lambda)$ and $\overline{(x-\overline{x})^2}(\lambda)$.)
Together with the Am-events and lab measurements of the PIN-diode average quantum efficiency AvQE(λ) [3], the glass transparency $T_{glass}(\lambda)$, the distance of the Diode to the pulsers $d_{Diode-Pulser}$ and the collection area of the diode A_{Diode}, the light flux at the PIN-diode can then be obtained via[4].

$$\overline{N}_{PhE}^{Diode}(\lambda) = 16570 \cdot \frac{Q_\mu^{Diode}(\lambda)}{Q_\mu^{Am}} \tag{23}$$

$$\frac{\Delta N_{PhE}^{Diode}(\lambda)}{\overline{N}_{PhE}^{Diode}(\lambda)} = \Big(\frac{\Delta Q_\mu^{Diode}(\lambda)}{Q_\mu^{Diode}} \oplus \frac{\Delta Q_\mu^{Am}}{Q_\mu^{Am}} \Big) \tag{24}$$

The two relative errors in eq. (24) should be very small assuming that the distributions are indeed Gaussian to good approximation. From these fits, one can then obtain the total fluence of light observed at the PIN-diode:

$$\Phi^{Diode}(\lambda) = \frac{\overline{N}_{PhE}^{Diode}(\lambda)}{T_{glass}^{Diode}(\lambda) \cdot AvQE(\lambda) \cdot A_{Diode}} \tag{25}$$

$$\frac{\Delta\Phi^{Diode}(\lambda)}{\Phi^{Diode}(\lambda)} = \Big(\frac{\Delta N_{PhE}^{Diode}(\lambda)}{N_{PhE}^{Diode}(\lambda)} \oplus \frac{\Delta T_{glass}^{Diode}(\lambda)}{T_{glass}^{Diode}(\lambda)} \oplus \frac{\Delta AvQE^{Diode}(\lambda)}{AvQE^{Diode}(\lambda)} \oplus \frac{\Delta A^{Diode}(\lambda)}{A^{Diode}(\lambda)} \Big) \tag{26}$$

[3]Note that in [2], the parameter λ means the wavelength corresponding to the emission spectrum of *one* certain-coloured LED, which then yields an AvQE. In our case, we have to take into account that three different colours are delivered which give AvQE(370nm),AvQE(460nm) and AvQE(520nm), respectively.

[4]In this and the following equations, the $\oplus$ sign means terms to be added quadratically, i.e. $a \oplus b \equiv \sqrt{a^2 + b^2}$.

The second error in eq. (26) concerning the PIN-diode glass transparency is difficult to judge. We expect to obtain 0.5%. However, dust and other environmental influences may decrease the transparency considerably. It is feasible to observe this effect by monitoring a long-term decrease of $Q_\mu^{Diode}(\lambda)$. The decrease would then be uncorrelated to a change in $Q_\mu^{b.p.}$ (see next item), but instead to environmental circumstances (storms, freeze, etc.) (see also section (6)). Such an increase has to be disentangled from effects of the LED ageing and a decrease of the transparency of the diffuser glass situated just above the diodes. Otherwise, the glass transparency should be measured again from time to time.

The average quantum efficiency is obtained by folding the spectrum of an LED of a given colour into the wavelength-dependent quantum efficiency of the PIN-diode. The last part known to a better precision than 0.1% for green and blue light and about 1% for UV [10]. The spectrum of the LEDs was measured by a continuous light source and is known to about 1%. However, in pulsed the spectrum may be different and needs to be measured again. The area of the PIN-diode is exactly 1 cm^2 and has a negligible error.

$$\Phi_{Diode}^{Camera}(\lambda) = \Phi^{Diode}(\lambda) \cdot \frac{d^2_{Diode-Pulser}}{d^2_{Camera-Pulser}} \tag{27}$$

$$\frac{\Delta\Phi_{Diode}^{Camera}(\lambda)}{\Phi_{Diode}^{Camera}(\lambda)} = \left(\frac{\Delta\Phi^{Diode}(\lambda)}{\Phi^{Diode}(\lambda)} \oplus \frac{2 \cdot \Delta d_{Diode-Pulser}}{d_{Diode-Pulser}} \oplus \frac{2 \cdot \Delta d_{Camera-Pulser}}{d_{Camera-Pulser}} \right) \tag{28}$$

The two distances in eq. (28) are still need to be measured and depend on the focusing position of the camera.

Blind pixel: This PMT will receive a highly reduced flux of photons with the aim to resolve the single Gaussians. In principle, it should be fitted to eq. (6). However, only the first electron peak can be resolved and none of the consequent ones. In addition, one has to properly take into account the lack of electrons which are lost due to backscattering from the first dynode. Therefore, a stepwise fitting procedure is planned: First fit only the pedestal, later the first peak from before the maximum to just after the peak subtracting the corresponding part obtained by the pedestal fit. It would however be desirable to develop a combined fit which takes into account all of the above mentionned effects.

For a flux measurement, only $Q_\mu^{b.p.}(\lambda)$ and $\Delta Q_\mu^{b.p.}(\lambda)$ are needed. However, the other values have to obey certain relations which can be used for cross-checks:

1. $\sigma_k^2 = k \cdot (\sigma_1^2 - \sigma_0^2) + \sigma_0^2$
2. $F^{lab.} = 1 + \frac{(\sigma_1^2(\lambda) - \sigma_0^2(\lambda))}{Q_1^2(\lambda)}$
3. Also the χ^2 of the fit will be monitored.

The derived flux at the position of the blind pixel can then be obtained together with the (known) average quantum efficiency of the PMT ($AvQE^{b.p.}(\lambda)$), the collection efficiency $\eta_{coll}^{b.p.}(U_{\mathsf{HV}})$, the transparency of the attenuation filter $T_{att}(\lambda)$ and the diaphragm of the PMT $A^{b.p.}_{geo}$ [5].

$$\Phi^{Camera}_{b.p.}(\lambda) = \frac{Q^{b.p.}_{\mu}(\lambda)}{AvQE^{b.p.}(\lambda) \cdot \eta^{b.p.}_{coll}(U_{\mathsf{HV}}) \cdot T_{att}(\lambda) \cdot A^{b.p.}_{geo}} \tag{29}$$

$$\frac{\Delta\Phi^{Camera}_{b.p.}(\lambda)}{\Phi^{Camera}_{b.p.}(\lambda)} = \Big(\frac{\Delta Q^{b.p.}_{\mu}(\lambda)}{Q^{b.p.}_{\mu}(\lambda)} \oplus \frac{\Delta AvQE^{b.p.}(\lambda)}{AvQE^{b.p.}(\lambda)} \oplus \frac{\Delta\eta^{b.p.}_{coll}(U_{\mathsf{HV}})}{\eta^{b.p.}_{coll}(U_{\mathsf{HV}})} \oplus \frac{\Delta T^{b.p.}_{att}(\lambda)}{T^{b.p.}_{att}(\lambda)} \oplus \frac{\Delta A^{b.p.}_{geo}}{A^{b.p.}_{geo}} \Big) \tag{30}$$

From the above errors, $\frac{\Delta AvQE^{b.p.}(\lambda)}{AvQE^{b.p.}(\lambda)} \lesssim 1.2\%$ ([7]). The measurements performed in [7] obtained the quantity:

$$\frac{QE^{PMT}(\lambda)}{QE^{REF}(\lambda)} = \frac{N^{PMT}_{Phe}(\lambda)}{N^{REF}_{Phe}(\lambda)} \tag{31}$$

The EMI-9116A photomultiplier was thereby short-circuited to all dynodes, i.e. the real quantum efficiency was measured without any contribution of $\eta^{b.p.}_{coll}(U_{\mathsf{HV}})$. Therefore, an additional estimate of this term is needed. For the EMI-9116A, we estimate $95 \pm 3\%$ [9]. $T^{b.p.}_{att}(\lambda)$ is known to about 0.1% according to the filter data-sheet and $A^{b.p.}_{geo}$ will be measured to an error smaller than this. The leading error comes thus from $AvQE^{b.p.}(\lambda)$, but again, environmental influences may cause changes in $T^{b.p.}_{att}(\lambda)$ and the corresponding effects must be monitored.

Combining the flux measurements: Naively, a combination of two independent flux-measurements with well-defined errors is performed via an arithmetic mean weighted with the inverse of the variances. We can thus define a mean fluence at the camera $\overline{\Phi}^{Camera}$:

$$\overline{\Phi}^{Camera} = \frac{\Delta\Phi^2_{b.p.} \cdot \Phi_{Diode} + \Delta\Phi^2_{Diode} \cdot \Phi_{b.p.}}{\Delta\Phi^2_{b.p.} + \Delta\Phi^2_{Diode}} \tag{32}$$

$$\frac{\Delta\overline{\Phi}^{Camera}}{\overline{\Phi}^{Camera}} = \frac{(\Phi_{b.p.} + \Phi_{Diode}) \cdot \Delta\Phi^2_{b.p.} \cdot \Delta\Phi^2_{Diode}}{\Delta\Phi^2_{b.p.} \cdot \Phi_{Diode} + \Delta\Phi^2_{Diode} \cdot \Phi_{b.p.}} \tag{33}$$

The "well-calibrated" PMTs: 18 "well-calibrated" PMTs should be located at the corners of the hexagon on three equally-distanced rings [6]. From these PMTs, the excess-noise factor $F^{w.c.}$ and the quantum efficiency is known with great precision from lab measurements. The events must be fitted to a Gaussian and yield: $Q^{w.c.}_{\mu}$, $\Delta Q^{w.c.}_{\mu}$, $\sigma^{w.c.}_{Q}$, $\Delta\sigma^{w.c.}_{Q}$, $A^{w.c.}$, $\Delta A^{w.c.}$, $\chi^{2\ w.c.}$. From these values, one can derive directly (Q_0 and σ_0 are obtained from the pedestal runs):

$$\overline{N}_{PhE} = F^{lab} \cdot \frac{(Q^{w.c.}_{\mu} - Q^{w.c.}_{0})^2}{\sigma^{2\ w.c.}_{Q} - \sigma^{2\ w.c.}_{0}} \tag{34}$$

$$\frac{\Delta N_{PhE}}{\overline{N}_{PhE}} = \Big(\frac{\Delta F^{lab}}{F^{lab}} \oplus \frac{2(\Delta Q^{w.c.}_{\mu} \oplus \Delta Q^{w.c.}_{0})}{Q^{w.c.}_{\mu} - Q^{w.c.}_{0}} \oplus \frac{2(\Delta\sigma^{w.c.}_{Q} \oplus \Delta\sigma^{w.c.}_{0})}{\sigma^{2\ w.c.}_{Q} - \sigma^{2\ w.c.}_{0}} \Big) \tag{35}$$

$$C_{PhE} = \frac{\overline{N}_{PhE}}{Q^{w.c.}_{\mu} - Q^{w.c.}_{0}} = F^{lab} \cdot \frac{Q^{w.c.}_{\mu} - Q^{w.c.}_{0}}{\sigma^{2\ w.c.}_{Q} - \sigma^{2\ w.c.}_{0}} \tag{36}$$

$$\frac{\Delta C_{PhE}}{C_{PhE}} = \Big(\frac{\Delta Q^{w.c.}_{\mu} \oplus \Delta Q^{w.c.}_{0}}{Q^{w.c.}_{\mu} - Q^{w.c.}_{0}} \oplus \frac{\Delta N_{PhE}}{\overline{N}_{PhE}} \Big) \tag{37}$$

[5] As stated in [2], there is practically no LONS contribution to this measurement. He expected $\sim (15-25) \cdot T_{att}$ photons which should give not more than $\sim 0.1 \cdot AvQE^{b.p.}$ per trigger.

Additionally, the $\overline{C}_{Phe}$ for all three wavelengths should agree within the statistical errors.

Knowing $\overline{C}_{Phe}$, $\overline{C}_{\gamma}$ (see below), $QE(\lambda)$ and a rough guess for η_{coll} one can then calibrate η_W for these PMTs.

Each PMT: Just like the "well-calibrated" ones, these PMTs must be fitted to a Gaussian and give: Q_{μ}^{PMT}, ΔQ_{μ}^{PMT}, σ_Q^{PMT}, $\Delta\sigma_Q^{PMT}$, A^{PMT}, ΔA^{PMT}, $\chi^{2\ PMT}$. The calibration then consists of the following steps:

1. *Calculate the expected number of photons:* Using the geometric area of the Winston cone A_{geo}^W, one can calculate:

$$N_{\gamma}(\lambda) = \overline{\Phi}^{Camera}(\lambda) \cdot A_{geo}^W \tag{38}$$

$$\frac{\Delta N_{\gamma}(\lambda)}{N_{\gamma}(\lambda)} = \Big(\frac{\Delta\overline{\Phi}^{Camera}(\lambda)}{\overline{\Phi}^{Camera}(\lambda)} \oplus \frac{\Delta A_{geo}^W}{A_{geo}^W} \Big) \tag{39}$$

2. *Calculate the conversion factor:*

$$C_{\gamma}^{calib}(\lambda) = \frac{Q_{\mu}^{PMT}(\lambda) - Q_0^{PMT}}{\overline{N}_{\gamma}(\lambda)} \tag{40}$$

$$\frac{\Delta C_{\gamma}^{calib}(\lambda)}{C_{\gamma}^{calib}(\lambda)} = \Big(\frac{\Delta N_{\gamma}(\lambda)}{N_{\gamma}(\lambda)} \oplus \frac{\Delta Q_{\mu}^{PMT}(\lambda) \oplus \Delta Q_0^{PMT}}{Q_{\mu}^{PMT}(\lambda) - Q_0^{PMT}} \Big) \tag{41}$$

$$C_{\gamma}^{corr}(\lambda) = \frac{(Q_{\mu}^{PMT}(\lambda) - Q_0^{PMT})}{\overline{N}_{\gamma}(\lambda)} \cdot S^{corr}(\lambda) \tag{42}$$

$$\frac{\Delta C_{\gamma}^{calib}(\lambda)}{C_{\gamma}^{calib}(\lambda)} = \Big(\frac{\Delta N_{\gamma}(\lambda)}{N_{\gamma}(\lambda)} \oplus \frac{\Delta Q_{\mu}^{PMT}(\lambda) \oplus \Delta Q_0^{PMT}}{Q_{\mu}^{PMT}(\lambda) - Q_0^{PMT}} \oplus \frac{\Delta S^{corr}(\lambda)}{S^{corr}(\lambda)} \Big) \tag{43}$$

3. *Calculate the excess noise:* This is done with the following formula:

$$F_{tot}^{calib}(\lambda) = \overline{N}_{\gamma}(\lambda) \cdot \frac{\sigma_Q^2}{(Q_{\mu}^{PMT} - Q_0^{PMT})^2} \tag{44}$$

$$\frac{\Delta F_{tot}^{calib}(\lambda)}{F_{tot}^{calib}(\lambda)} = \Big(\frac{\Delta\overline{N}_{\gamma}}{\overline{N}_{\gamma}} \oplus \frac{2\Delta\sigma_Q}{\sigma_Q} \oplus \frac{2(\Delta Q_{\mu}^{PMT} \oplus \Delta Q_0^{PMT})}{Q_{\mu}^{PMT} - Q_0^{PMT}} \Big) \tag{45}$$

   For the "well-calibrated" PMTs, F_{tot} has to be cross-checked with F_{PMT} delivered from the lab measurements.

4. *Calculate the number of photons from a measured value of Q_{μ}:*
   The conversion factor C_{γ} and the excess noise factor F_{tot} can then be used to calculate from one given (integrated) amplitude back to the *mean number of photons expected from a certain*

wavelength and the expected fluctuations. For a given shower event the number of expected photons is:

$$\overline{N}_\gamma^{\,corr}(\lambda) = \frac{Q_\mu^{PMT} - Q_0^{PMT}}{\overline{C}_\gamma^{\,calib}(\lambda)\cdot S^{\,corr}} \tag{46}$$

$$\begin{aligned}
\frac{\Delta\overline{N}_\gamma^{\,corr}(\lambda)}{\overline{N}_\gamma^{\,corr}(\lambda)} &= \frac{\Delta C_\gamma(\lambda)}{C_\gamma(\lambda)} \oplus \frac{\Delta(Q_\mu^{PMT} - Q_0^{PMT})}{Q_\mu^{PMT} - Q_0^{PMT}} \oplus \frac{\Delta S^{\,corr}}{S^{\,corr}} \\
&= \frac{\Delta C_\gamma(\lambda)}{C_\gamma(\lambda)} \oplus \sqrt{\frac{F_{tot}^{calib}}{N_\gamma^{calib}}}\cdot\left(1 + \frac{\Delta F_{tot}^{calib}(\lambda)}{2F_{tot}(\lambda)}\right) \oplus \sqrt{\mathsf{var}(\eta_{tot}^{corr})} \\
&= \frac{\Delta C_\gamma(\lambda)}{C_\gamma(\lambda)} \oplus \sqrt{\frac{F_{tot}^{calib}\cdot\left(1 + \frac{\Delta F_{tot}^{calib}(\lambda)}{F_{tot}^{calib}(\lambda)}\right)}{S^{\,corr}\cdot N_\gamma^{corr}} + \mathsf{var}(\eta_{tot}^{corr})} \qquad (47) \\
&\equiv \frac{\Delta C_\gamma(\lambda)}{C_\gamma(\lambda)} \oplus \sqrt{\frac{F_{tot}^{air\ sh}}{N_\gamma^{corr}}} \qquad (48)
\end{aligned}$$

Here we have used eq. (21) to obtain eq. (48) from eq. (47). Note that for a lack of calibration of $F_{tot}^{air\ sh}$, one has to calculate with eq. (47).

3 The Calibration Scripts

We propose to use different configuration scripts which can be addressed (and modified) either by the central control or by single users. Such a script has a predefined and simple syntax. A complete calibration should run every beginning of the night and running reduced calibrations (without linearity and reduced continuous light source calibration) at certain intervals (e.g. every hour). E.g. the configuration script for the complete calibration is given in the appendix B. which needs about 13 minutes, but the typical trigger frequency of 500 Hz can most probably be increased. Analogously, a script is needed which describes the calibration before each run (e.g. PIN-diode and Pulser), the pedestals during the runs and perhaps some special treatment for the continuous light calibration only.

The scripts are flexible and can be modified at any time. The calibration control subsystem interprets the script and proceeds by steering the trigger and the calibration driver or returns an error message if the script cannot be interpreted correctly.

4 Data Flow

The calibration scripts are included in the software for the calibration subsystem of the Central Control. The Central Control itself decides to carry out a calibration run and which configuration script to use. It then calls the calibration subsystem for execution of the script which controls the triggers and the calibration hardware and handles errors. Three trigger flags will be used:

1. Am-241 PIN-diode trigger
2. Pedestal trigger
3. Other calibration (pulse LEDs or coninuous light source)

Additionally, the 24 bits characterizing the calibration (16 bits for the 16 pulse LED slots, 8 bits for the strength of the continuous light source) will be written into 2 of the Digital Modules (DMs) situated in the FADC motherboard. Each of these DMs has 16 bits input.

To figure out later what has been done, additionally the time stamp can be used together with the single steps of the calibration subsystem stored in a local log-file. Note however that the Central Control computer clock is not precisely synchronized with the GPS (DAQ) (up to an error of $\sim$50 ms). For the flat-fielding, the DAQ itself will provide a fast routine using the information coming from the DMs. In order to match LED slot with the corresponding colour LED, a general configuration file exists which will change with time only if hardware settings are modified inside the calibration box. A sketch of the planned data flow is shown in figure 2.

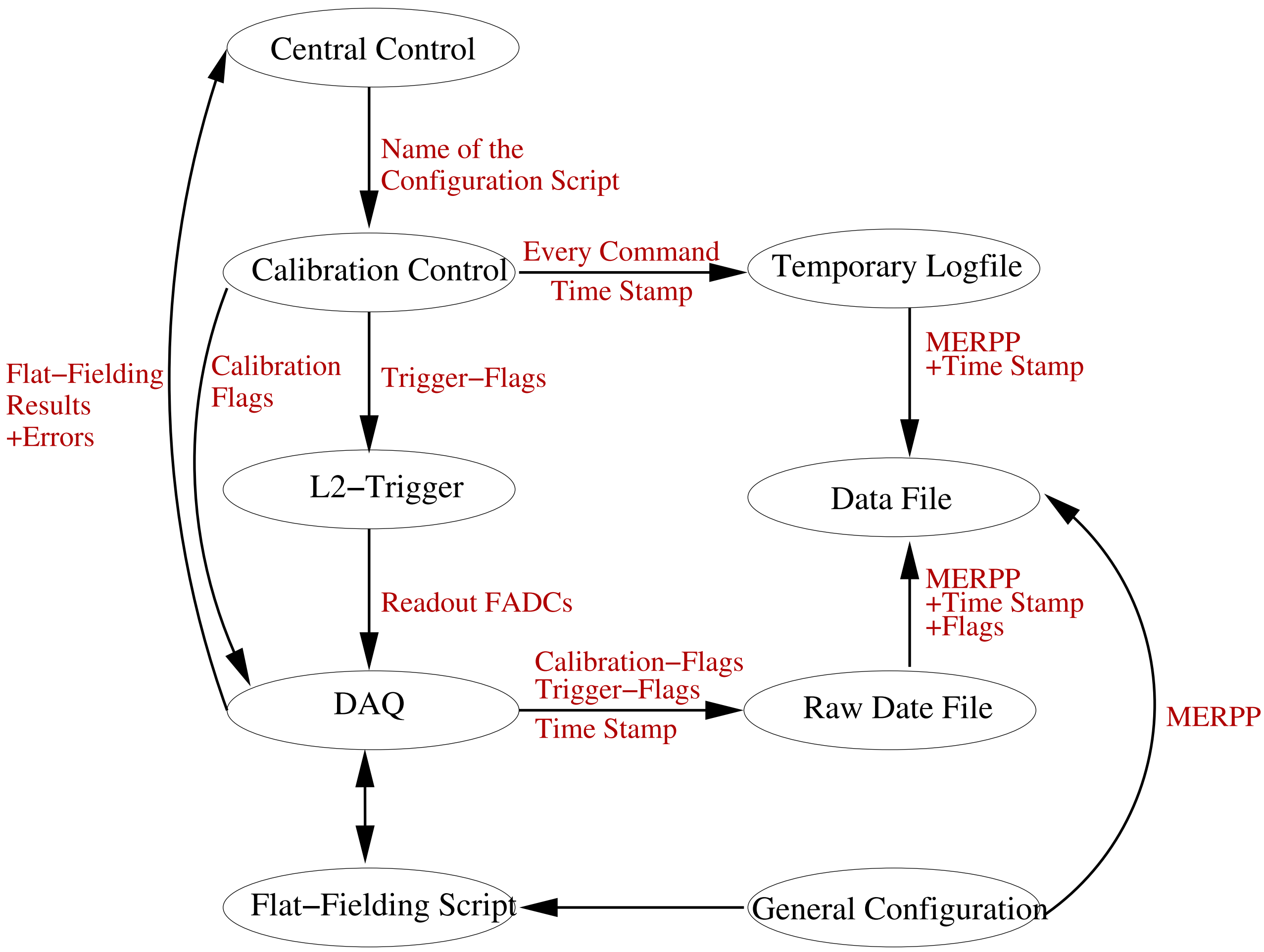

Figure 2: Data flow of the calibration information

5 Flatfielding

Experience with all previous Cherenkov telescopes has shown that the analysis enormously simplifies by "flat-fielding" the camera. Flat-fielding means that the dependency of $\overline{C}_{Phe}$ or $\overline{C}_\gamma$ on U_{HV} is exploited in such a way that the individual high-voltages of PMTs are adjusted such that all $\overline{C}_{Phe}$ or $\overline{C}_\gamma$ get the same value. In the CT1 telescope, flat-fielding was performed for photo-electrons, i.e. all $\overline{C}_{Phe}$ were adjusted. Equation 50 gives a very fast way to obtain the individual values:

$$\begin{aligned} F_{PMT}(U_{\mathsf{HV}}) = 1 + \mathsf{var}(G(U_{\mathsf{HV}})) &= \eta_{tot}(\lambda, \theta = 0) \cdot F_{tot}(\lambda, U_{\mathsf{HV}}, \theta = 0) - \frac{\mathsf{var}(A)}{\overline{G}(U_{\mathsf{HV}})} \\ &\approx \eta_{tot}(\lambda = \text{fix}, \theta = 0) \cdot F_{tot}(\lambda = \text{fix}, U_{\mathsf{HV}}, \theta = 0) \qquad (49) \\ \overline{N}_{PhE} &= \frac{F_{PMT}(U_{\mathsf{HV}})}{\mathsf{var}(Q)} \\ \overline{C}_{PhE} &= \frac{\overline{N}_{PhE}}{Q_\mu - Q_0} \qquad (50) \end{aligned}$$

Approximation 49 is however incorrect as soon as there is a different wavelength-dependency for different pixels. At the MAGIC software meeting [11] therefore the decision was taken to flat-field directly for $\overline{C}_\gamma$.

It is principally possible to flatfield for:

- $\overline{C}_\gamma^{air\ sh.}(\lambda, U_{\mathsf{HV}})$
- $\overline{C}_\gamma(\lambda, U_{\mathsf{HV}}, \theta = 0)$
- $\lambda = 460$nm (blue light)
- a zenith-dependent wavelength
- the wavelength folded into the probability distribution of λ

$$\overline{C}_{eff}(\vartheta) \equiv \int_{\lambda_{min}}^{\lambda^{max}} \overline{C}_\gamma(\lambda) \cdot P(\vartheta; \lambda)\, d\lambda \qquad (51)$$

with:

$$P(\vartheta; \lambda) = \int_{E^{min}}^{E^{max}} \int_0^{\delta^{max}} P(E) \cdot P(\delta) \cdot P(\delta, E, \vartheta, \lambda)\, dE\, d\delta \qquad (52)$$

with $P(E)$ being the probability for a shower with the energy E to trigger the camera (which depends on the incident energy spectrum), $P(\delta)$ the probability for an event of a certain impact parameter δ to trigger the camera (should not change with the source) and $P(\delta, E, \vartheta, \lambda)$ the probability distribution to obtain a photon with wavelength λ at a given shower energy E, impact parameter δ and zenith angle ϑ. One should test the robustness of $P(\vartheta; \lambda)$ with different energy spectra and check the magnitude of the overall wavelength-dependency of the flat-fielding with the corresponding changes induced by showers observed at different zenith angles in order to proceed further into this direction.

Certainly the last approach is the most sophisticated one (and thus the one which should correct best for systematic effects and thus improve most e.g. the energy resolution), but the magnitude of the effects has still to measured. In the beginning, flat-fielding will most reasonably be performed with blue light only.

6 Monitoring of the calibration behavior

We suggest to implement some floating average to monitor **short-term** variations for the following variables:

- The mean charge $Q_\mu^{PMT}(\lambda)$ and its sigma $\sigma_Q(\lambda)$.
- For possible outliers: $\frac{\overline{Q}^{PMT}}{Q_\mu^{PMT}}$ and $\frac{\overline{(Q-\overline{Q})^2}}{\sigma_Q^{2\ PMT}}$ (see also sect. 2).
- For different wavelengths: $\frac{Q_\mu^{PMT}(\lambda_i)}{Q_\mu^{PMT}(\lambda_j)}$ and $\frac{\sigma_Q^{PMT}(\lambda_i)}{\sigma_Q^{PMT}(\lambda_j)}$
- The pedestals Q_0^{PMT} and their sigma σ_0.
- For possible outliers: $\frac{\overline{Q}^{ped}}{Q_0^{ped}}$ and $\frac{\overline{(Q^{ped}-\overline{Q}^{ped})^2}}{\sigma_0^{2\ ped}}$

This part should montitor any fluctuations in the PMT/amplification behavior like oscillations, short-term failures, short-term excessive noise, bad connections, etc. Remember that the PMT currents are also monitored by the Central Control. This proposed additional monitoring scheme should provide some complementarity.

Moreover, we need to be sure that every step in the calibration scheme is correct and does not change with time. This is especially valid for numbers obtained from lab measurements. These will be monitored for **long-term** variations:

$T_{glass}^{Diode}(\lambda)$ and $T_{att}^{blind\ pixel}(\lambda)$: This number is measured in the lab together with a certain error, but may change due to external influences: rain, freeze, heat, dust, bacteria, etc. Although the PIN-diode box points downwards and is thus not directly exhibited to rain, changes will occur, most probably in a wavelength-dependent way.

$AvQE\ ^{Diode}(\lambda)$ and $AvQE\ ^{blind\ pixel}(\lambda)$: This part should be stable, and changes are most probably much smaller than those anticipated for $T_{glass}^{Diode}(\lambda)$. Anyway, the only number which enters the analysis, is the product $AvQE^{Diode}(\lambda) \cdot T_{glass}^{Diode}(\lambda)$.

The geometrical factors: areas, distances: They are not expected to change with time, not even in very bad weather conditions. What could perhaps be imagined, is a shift of the PIN-diode box out of the 4 degrees uniform light flux – e.g. for reasons of a change in the long term LED behaviour.

Lab measurements for the well-calibrated PMTs: This concerns above all $F_{w.c.}^{lab}$.

The calibration system has been designed in order to have a clear redundancy of calibration schemes. This feature will be exploited for monitoring. The flux of photons arriving at the camera is calculated in two equivalent ways (eq. (28) and eq. (30)) and should yield the same value in between the assumed errors.

We therefore suggest to implement some long-term floating average for the following variables:

- $Q_{\mu}^{b.p.}(\lambda)$, $Q_{\mu}^{Diode}(\lambda)$ and $< Q_{\mu}(\lambda) > \equiv \frac{1}{N_{PMT}} \sum_{i=0}^{N_{PMT}} Q_{\mu}^{i}(\lambda)$
- $\frac{F_{tot}^{w.c.}}{F_{lab}^{w.c.}}$
- $C_{\gamma}^{PMT}(\lambda)$, $F_{tot}^{PMT}(\lambda)$

Changes in these quantities are most probably due to changes in the PMT/amplification chain behaviour.

- Φ_{Diode}^{Camera}, $\Phi_{b.p.}^{Camera}$
- $\frac{\Phi_{Diode}^{Camera}}{\Phi_{b.p.}^{Camera}}$
- $\frac{Q_{\mu}^{b.p.}(\lambda_i)}{Q_{\mu}^{Diode}(\lambda_i)}$, $\frac{<Q_{\mu}>(\lambda_i)}{Q_{\mu}^{Diode}(\lambda_i)}$, $\frac{<Q_{\mu}>(\lambda_i)}{Q_{\mu}^{b.p.}(\lambda_i)}$

Changes in one of the above variables should pinpoint directly to a change in the "laboratory numbers", i.e. the calibration setup as such.

7 Conclusions

For the calibration of the CT1 telescope, $\overline{C}_{Phe}$ was used for the flat-fielding procedure. I.e. the gains of the individual PMTs were adjusted in a way that all $\overline{C}_{Phe}$ should give an equal value. Thus, observing a certain ADC distribution in the field of the camera, one could immediately calculate the corresponding mean photo-electron values and thus the energy estimator. Flat-fielding for photo-electrons thus means that the sum of charges $\sum_{i=0}^{N_{PMT}} Q^i_\mu$ becomes proportional to the energy of the shower. This approach however, introduces systematic errors since the quantum efficiencies between the PMTs differ as well as the response of the photo-multiplier to different incident wavelengths. *We therefore suggest to flat-field for photons.* Since air-showers contain a mixture of photon wavelengths and the pixel response is wavelenght-dependent, a flat-fielding procedure for "equivalent blue-light" photons is presented here and possible additions only afterwards. The photon wavelength of 460nm (blue light) which will be examined with the best accuracy (8 out of 16 slots in the calibration board will host blue LEDs) by the calibration system. Since the authors differ in their suggestions on the exact way to proceed, we shortly discuss here two possibilities.

Flat-field for C^{calib}_γ (460 nm) eq. (40): This approach assumes that the equivalent number of photons arriving under an angle $\cos(\theta) = 1$ is the only quantity correctly calibrated and monitored. Summing N^{calib}_γ does NOT yield something proportional to the incident total light flux since every pixel may have different values of S^{corr}, BUT comparing it to Monte-Carlo distributions (back-calibrated exactly the same way) should yield good comparability. Note that the distributions of $\eta\big(\cos(\theta), \phi, \lambda\big)$ will also be used as direct input into the Monte-Carlo simulations since other detailed measurements of $\eta_W(\theta, \phi)$ are not at hand. The advantage is that the distribution of incident light onto the mirror disk is simulated correctly in the Monte-Carlo. The drawback of this method is the loss of proportionality of the sum of charges to the total incident light flux.

Flat-field for C^{corr}_γ (460 nm) eq. (42): This means correcting for the total incident photon flux even if there is a systematic error in the assumption that photons arrive uniformly over the area of the mirror disk. Sums of measured charges Q^i_μ become proportional to the total incident light flux and thus the energy estimator. There is still a systematic difference due to the non-uniformity of incident light, however this error is smaller than the one obtained by neglecting the different incidence angles. If one performs the same back-correcting procedure with the MC simulation, one also gets comparable variables. The disadvantage of this procedure consists of the fact that it seems more complicated and less intuitive.

For a subsequent analysis, especially the energy estimation, a further incorporation of the wavelength dependency would be useful. However, without knowing the wavelength of the incident photon, the system is under-determined and cannot be solved. We will therefore suggest to extract the missing information from Monte-Carlo studies to obtain a distribution function of incident wavelengths from electro-magnetic showers $P(\vartheta, \lambda)$:

$$\overline{C}_{eff}(\vartheta) \equiv \int_{\lambda_{min}}^{\lambda^{max}} \overline{C}_\gamma(\lambda) \cdot P(\vartheta; \lambda)\, d\,\lambda$$

with:

$$P(\vartheta; \lambda) = \int_{E^{min}}^{E^{max}} \int_0^{\delta^{max}} P(E) \cdot P(\delta) \cdot P(\delta, E, \vartheta; \lambda)\, dE\, d\delta \tag{53}$$

with $P(E)$ being the probability for a triggering event with the energy E (which depends on the incident energy spectrum), $P(\delta)$ the probability for an event of a certain impact parameter δ (should not change with the source) and $P(\delta, E, \vartheta, \lambda)$ the probability distribution to obtain a photon with wavelength λ at a given energy E, impact parameter δ and zenith angle ϑ. One should test the robustness of $P(\vartheta; \lambda)$ with different energy spectra and check the magnitude of the overall wavelength-dependency of calibration with the corresponding changes induced by showers observed at different zenith angles in order to proceed further into this direction.

The calibration box is situated in the middle of the mirror disk, therefore the incident angle θ is always the same under which the photons arrive. In order to get a more precise estimate about $\mathsf{var}\big(\eta_{tot}(\theta, \phi, \lambda)\big)$, we need light sources under variable incident angles. This could be done by simply installing several additional calibration boxes at the edges of the mirror disk with the disadvantage that again, only certain angles are picked out for calibration. Another possibility consists of installing a powerful light source (which could then be a continuous light source) at the Roque de los Muchachos and rotate the telescope w.r.t. all incident angles.

Acknoledgements

We thank Manel Martinez, Javier Lopez, Ernst-Jan Buis for detailed proof-reading.

References

[1] Th. Schweizer, M. Gaug, Talks presented at the MAGIC Internal meeting, Barcelona, Feb. 3^{rd}-5^{th}

[2] Th. Schweizer et al., The Optical Calibration of the MAGIC Telescope Camera, To be published in "Transactions on Nuclear Science TNS", IEEE Conf., San Diego, Nov. 2001

[3] H. Kornmayer, W. Wittek, Pixel calibration, event preprocessing, physics analysis, TDAS-00-05,000303.

[4] D.Bastieri et et al., A two-level pattern trigger for the MAGIC telescope, TDAS-00-12, 000520.

[5] R. Mirzoyan, Conversion Factor Calibration for MAGIC Based On the Use of Measured F-Factors of PMTs, TDAS-00-15,010412.

[6] R. Mirzoyan, Talk presented at the MAGIC Internal meeting in Barcelona, Feb. 3^{rd}-5^{th}.

[7] D. Paneque, presentation given at the MAGIC meeting, Barcelona

[8] D. Paneque, An optical properties studies of the new hemispherical PMTs from Electron Tubes, Diploma thesis, 2001.

[9] S. Ostankov, private communication

[10] National Institute of Standard and Technologies (NIST), Spectroradiometric Detector Measurements: Ultraviolet Detectors and Visible to Near-Infrared Detectors, http://ois.nist.gov/sdm/

[11] Minutes of the Software meeting Barcelona 27-29 June, 2002
http://hegra1.mppmu.mpg.de/MAGIC/private/minutes/sw-meeting-270602/minutes.html

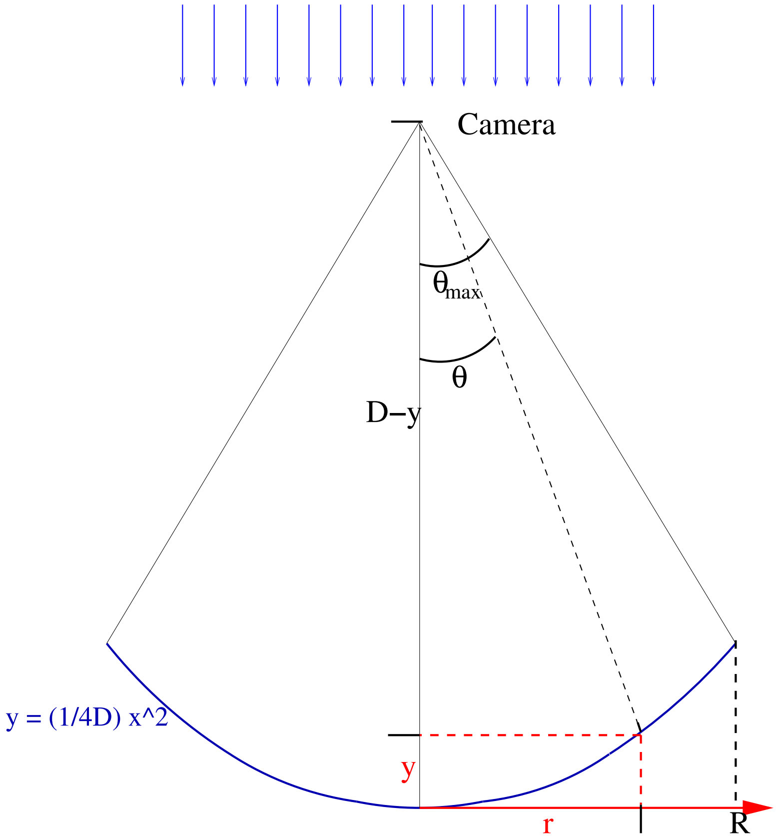

Figure 3: Schematics of the telescope geometry

A The probability distribution of photon incident angles onto the Winston cones for uniform air shower light

Assume uniform light arriving parallel to the telescope axis under an impact parameter r (see fig 3). Because of the growing mirror area, the phase space for photons arriving at high r is much bigger than for small radii. Thus, a probability distribution function $P(r)dr$ can be defined:

$$P(r)dr = \begin{cases} \frac{r}{\pi R^2} dr & 0 < r < R \\ 0 & R < r \end{cases} \tag{54}$$

Eq. (54) like all following probability distributions is normalized to $\frac{1}{2\pi}$ and runs from 0m to $R = 8.5$m which is the outer radius of the mirror disk.

The impact parameter transforms into an incident angle onto the Winston cone with the relation:

$$\begin{aligned}
\tan(\theta) &= \frac{r}{D-y} \\
&= \frac{r}{D-\frac{r^2}{4D}} \\
\cos(\theta) &= \frac{4D^2-r^2}{4D^2+r^2} && (55) \\
\cos(\theta_{max}) &= \frac{4D^2-R^2}{4D^2+R^2} && (56)
\end{aligned}$$

where we have used the fact that the camera is situated in the focal point of the mirror parabola at a distance $D \approx 17$m from the central mirror. The variable $\theta_{max} \approx 28°$ is the maximum angle under which light can arrive onto the Winston cone.
Eq. (55) can be solved for r and yields:

$$r(\cos(\theta)) = 2D\sqrt{\frac{1-\cos(\theta)}{1+\cos(\theta)}} \qquad (57)$$

$$\frac{dr}{d\cos(\theta)} = -2D\sqrt{\frac{1+\cos(\theta)}{1-\cos(\theta)}} \cdot \frac{2}{(1+\cos(\theta))^2} \qquad (58)$$

Together with eq. (54), we obtain a probability function for incident angles onto the camera which depends only on the geometry of the telescope:

$$P(r)dr = P\big(r(\cos(\theta))\big)d\cos(\theta) \cdot \frac{dr}{d\cos(\theta)} \qquad (59)$$

$$P\big(r(\cos(\theta))\big) \cdot \frac{dr}{d\cos(\theta)} \equiv P(\cos(\theta)) = \begin{cases} 0 & \frac{4D^2-R^2}{4D^2+R^2} > \cos(\theta) \\ \frac{-4D^2}{\pi R^2} \cdot \frac{1}{(1+\cos(\theta))^2} & 1 > \cos(\theta) > \frac{4D^2-R^2}{4D^2+R^2} \end{cases} \qquad (60)$$

B Example of a configuration script

```
#define ON  1
#define OFF 0

#define NONE      0000000000000000

#define BLUE_01   1000000000000000
#define BLUE_02   0100000000000000
#define BLUE_03   1100000000000000
#define BLUE_04   0010000000000000
#define BLUE_05   1010000000000000
#define BLUE_06   0110000000000000
#define BLUE_07   1110000000000000
#define BLUE_08   0001000000000000
#define BLUE_09   1001000000000000
#define BLUE_10   0101000000000000
#define BLUE_11   1101000000000000
#define BLUE_12   0011000000000000
#define BLUE_13   1011000000000000
#define BLUE_14   0111000000000000
#define BLUE_15   1111000000000000
#define BLUE_16   0001100000000000
#define BLUE_17   1001100000000000
#define BLUE_18   0101100000000000
#define BLUE_19   1101100000000000
#define BLUE_20   0011100000000000
#define BLUE_21   1011100000000000
#define BLUE_22   0111100000000000
#define BLUE_23   1111100000000000
#define BLUE_24   0001110000000000
#define BLUE_25   1001110000000000
#define BLUE_26   0101110000000000
#define BLUE_27   1101110000000000
#define BLUE_28   0011110000000000
#define BLUE_29   1011110000000000
#define BLUE_30   0111110000000000
#define BLUE_31   1111110000000000
#define BLUE_32   0001111000000000
#define BLUE_33   1001111000000000
#define BLUE_34   0101111000000000
#define BLUE_35   1101111000000000
#define BLUE_36   0011111000000000
#define BLUE_37   1011111000000000
#define BLUE_38   0111111000000000
#define BLUE_39   1111111000000000
```

```
#define BLUE_40   0001111100000000
#define BLUE_41   1001111100000000
#define BLUE_42   0101111100000000
#define BLUE_43   1101111100000000
#define BLUE_44   0011111100000000
#define BLUE_45   1011111100000000
#define BLUE_46   0111111100000000
#define BLUE_47   1111111100000000

#define BLUE_ALL  1111111100000000

#define UV_01     0000000010000000
#define UV_02     0000000001000000
#define UV_03     0000000011000000
#define UV_04     0000000000100000
#define UV_05     0000000010100000
#define UV_06     0000000001100000
#define UV_07     0000000011100000
#define UV_08     0000000000110000
#define UV_09     0000000010110000
#define UV_10     0000000001110000
#define UV_11     0000000011110000

#define UV_ALL    0000000011110000

#define GREEN_01  0000000000001000
#define GREEN_02  0000000000000100
#define GREEN_03  0000000000001100
#define GREEN_04  0000000000000010
#define GREEN_05  0000000000001010
#define GREEN_06  0000000000000110
#define GREEN_07  0000000000001110
#define GREEN_08  0000000000000011
#define GREEN_09  0000000000001011
#define GREEN_10  0000000000000111
#define GREEN_11  0000000000001111

#define GREEN_ALL 0000000000001111

/* TRAIN-FREQ NR-OF-EVTS  FREQ.  MODUL      PEDESTAL    CONT.LIGHT-SRC
      (HZ)                (HZ)   -PATTERN  (ON=1/OFF=0)  (0-256)    */

/* PIN-DIODE CALIBRATION */
       0       10000      500      NONE       ON            OFF
/* LED-MODULES */
       0       20000      500      BLUE_ALL   OFF           OFF
       0       20000      500      UV_ALL     OFF           OFF
```

```
       0       20000      500      GREEN_ALL  OFF          OFF
/* PIN-DIODE CALIBRATION */
       0       1000       500      NONE       ON           OFF
/* LINEARITY CALIBRATION */
       0       10000      500      BLUE_01    OFF          OFF
       0       10000      500      BLUE_02    OFF          OFF
       0       10000      500      BLUE_04    OFF          OFF
       0       10000      500      BLUE_08    OFF          OFF
/* PIN-DIODE CALIBRATION */
       0       1000       500      NONE       ON           OFF
/* LINEARITY CALIBRATION CONT. */
       0       10000      500      BLUE_12    OFF          OFF
       0       10000      500      BLUE_16    OFF          OFF
       0       10000      500      BLUE_20    OFF          OFF
       0       10000      500      BLUE_24    OFF          OFF
       0       10000      500      BLUE_28    OFF          OFF
/* PIN-DIODE CALIBRATION */
       0       1000       500      NONE       ON           OFF

/* TRAIN-FREQ NR-OF-EVTS  FREQ.  MODUL      PEDESTAL    CONT.LIGHT-SRC
      (HZ)                (HZ)   -PATTERN  (ON=1/OFF=0)   (0-256)  */
/* LINEARITY CALIBRATION CONT. */
       0       10000      500      BLUE_32    OFF          OFF
       0       10000      500      BLUE_36    OFF          OFF
       0       10000      500      BLUE_42    OFF          OFF
       0       10000      500      BLUE_46    OFF          OFF
       0       10000      500      BLUE_ALL   OFF          OFF
/* PIN-DIODE CALIBRATION */
       0       1000       500      NONE       ON           OFF
/* CONTINUOUS LIGHT SOURCE */
       0       10000      500      NONE        1            1
       0       10000      500      NONE        1            2
       0       10000      500      NONE        1            4
       0       10000      500      NONE        1            6
       0       10000      500      NONE        1            8
/* PIN-DIODE CALIBRATION */
       0       1000       500      NONE       ON           OFF
/* CONTINUOUS LIGHT SOURCE CONT. */
       0       10000      500      NONE        1            10
       0       10000      500      NONE        1            12
       0       10000      500      NONE        1            16
       0       10000      500      NONE        1            20
       0       10000      500      NONE        1            24
/* PIN-DIODE CALIBRATION */
       0       1000       500      NONE       ON           OFF
/* CONTINUOUS LIGHT SOURCE CONT. */
       0       10000      500      NONE        1            28
```

```
       0       10000      500      NONE        1            32
       0       10000      500      NONE        1            38
       0       10000      500      NONE        1            44
       0       10000      500      NONE        1            50
/* PIN-DIODE CALIBRATION */
       0       1000       500      NONE       ON           OFF
/* CONTINUOUS LIGHT SOURCE CONT. */
       0       10000      500      NONE        1            56
       0       10000      500      NONE        1            64
       0       10000      500      NONE        1            72
       0       10000      500      NONE        1            80
       0       10000      500      NONE        1            88
/* PIN-DIODE CALIBRATION */
       0       1000       500      NONE       ON           OFF
/* CONTINUOUS LIGHT SOURCE CONT. */
       0       10000      500      NONE        1            100
       0       10000      500      NONE        1            112
       0       10000      500      NONE        1            128
       0       10000      500      NONE        1            144
       0       10000      500      NONE        1            160
/* PIN-DIODE CALIBRATION */
       0       1000       500      NONE       ON           OFF
/* CONTINUOUS LIGHT SOURCE CONT. */
       0       10000      500      NONE        1            178
       0       10000      500      NONE        1            194
       0       10000      500      NONE        1            210
       0       10000      500      NONE        1            230
       0       10000      500      NONE        1            256
```

C What is still needed from lab measurements?

1. For the blind pixel:
   - The wavelength-dependent transparency of the attenuation filter
   - The excess noise factor of the blind pixel PMT
   - The collection efficiency of the blind pixel PMT
2. For the PIN-diode:
   - The wavelength-dependent transparency of the glass housing
   - The average quantum efficiency in pulsed mode
3. For the LEDs:
   - The pulser LED spectra of each color $I(\lambda)$.
4. For the "well-calibrated" PMTs:
   - The excess noise factor F and a realistic assumption about the error ΔF.
   - The AvQE(λ)
   - A good estimate about $\eta_{coll}(\lambda)$
5. For the continuous light source measurement:
   - The electronic noise σ_0 of the amplification chain
6. For each PMT:
   - The angle-dependent light collection efficiency $\eta\big(\cos(\theta,\phi)\big)$